2004

Analysis of inelastic interactions for therapeutic proton beams using Monte Carlo simulation

Anatoly B. Rosenfeld
University of Wollongong, anatoly@uow.edu.au

A. J. Wroe
University of Wollongong

I. Cornelius
University of Wollongong, iwan@uow.edu.au

M. Reinhard
ANSTO, Australia

D. Alexiev
ANSTO, Australia

Analysis of Inelastic Interactions for Therapeutic Proton Beams Using Monte Carlo Simulation

Anatoly B. Rosenfeld, *Senior Member, IEEE*, Andrew J. Wroe, Iwan M. Cornelius, *Member, IEEE*, Mark Reinhard, *Member, IEEE*, and Dimitri Alexiev, *Member, IEEE*

***Abstract*—The irradiation of various tissue-like materials by therapeutic proton beams was simulated using Monte Carlo. The contribution of inelastic reaction products to the depth-dose distribution was determined. The use of silicon microdosimeters for verifying Monte Carlo calculations was also investigated. The importance of these studies to Monte Carlo-based treatment planning systems is emphasized.**

I. Introduction

PROTON therapy is offering highly conformal radiotherapy treatment, which is based on specific properties of depth-dose deposition by energetic protons in a medium. The energies of protons utilized in proton therapy are around 60 MeV for the treatment of eye tumors and up to 250 MeV for deep-seated tumors.

For accurate conformal treatment of the target volume, it is important to have treatment-planning systems that are able to simulate precisely the interaction of the primary proton beam within the body. Taking into account an electron density distribution in a target volume obtained from a CT scan, the CT numbers may not be adequate for the planning of heterogeneous targets. Errors in the dose distribution and proton range can be encountered for different target materials if proton inelastic reactions are not considered as part of the absorbed dose simulations [1]. Dose planning systems based on Monte Carlo simulations would be optimal for calculating dose distributions in heterogeneous targets if the composition of the target is known.

Recently, several groups have studied Monte Carlo approaches for dose planning in proton therapy. A simplified Monte Carlo approach was proposed for dose planning in heterogeneous targets [2]. However, verification of this plan was achieved by the conversion of doses in a body to the dose distribution in water with verification of the latter. It was demonstrated that the agreement between simulated and measured doses in water is not a guarantee of correct dose distribution within the body.

The dose distribution verification should be done in a phantom containing realistic heterogeneities. In many cases of proton therapy treatment, the highly conformal absorbed dose distributions do not guarantee the best treatment outcome particularly in case of the spread out Bragg peak (SOBP). It has been demonstrated that a variable radiobiological effect (RBE) could be implemented in a clinical proton treatment planning system, for use particularly when the target is close to critical organs [3]; however, further development of radiobiological models is required. This means that dose planning in proton therapy could be conducted utilizing an RBE-based Monte Carlo treatment planning system in a medium with well-known composition. Such a system would employ the appropriate radiobiological models when primary and secondary charged particle spectra are known.

In this paper, we investigate the importance of inelastic proton scattering on an absorbed dose distribution and proton ranges in different tissues using the GEANT4 Monte Carlo simulation kit. We also investigate the potential use of silicon microdosimetry for Monte Carlo verification, a technique that does not require tissue equivalence of the dosimeter.

II. Simulation of Absorbed Doses in a Proton Therapy Beam

Simulations were carried out for monoenergetic 60- and 200-MeV proton beams within homogeneous: water, A-150 tissue equivalent plastic, adipose (ICRP), bone (ICRP), and muscle (ICRP) phantoms. Each energy/tissue combination was first simulated neglecting inelastic scatter and then with the inclusion of inelastic scatter. A comparison between the depth-dose distributions for these scenarios provided important information on the importance of inelastic scatter interactions.

A. Simulation Parameters

The GEANT4 Monte Carlo Transport Toolkit (version 4.5.2) [4] was used to simulate depth-dose depositions within homogeneous phantoms. The phantom geometry consisted of a rectangular prism with sensitive slices covering the cross sectional area of the phantom (Fig. 1). The sensitive slices 5–10 μm in thickness were separated by gaps of 0.1–1 mm. The cross sectional area of the sensitive slices was 5×5 cm. This provides an adequate cross sectional area for pencil beam depth-dose distributions as well as for small area broad beams. In total, 320 sensitive slices were employed at regular intervals within the phantom to provide adequate resolution of the depth-dose distribution.

The inelastic scattering model employed in this investigation was the G4PreCompound model and is considered suitable for the therapeutic energy range [5]. The G4PreCompound model accounts for the production of secondary particles as a result of inelastic scatter, including the generation of charged secondaries, neutrons, and photons. The elemental composition, and

Manuscript received November 17, 2003; revised June 27, 2004 and August 9, 2004. This work was supported in part by the Australian Institute of Nuclear Science and Engineering.

A. B. Rosenfeld, A. J. Wroe, and I. M. Cornelius are with the University of Wollongong, Wollongong NSW 2522, Australia (e-mail: anatoly@uow.edu.au).

M. Reinhard and D. Alexiev are with the Australian Nuclear Science and Technology Organization.

Digital Object Identifier 10.1109/TNS.2004.839072

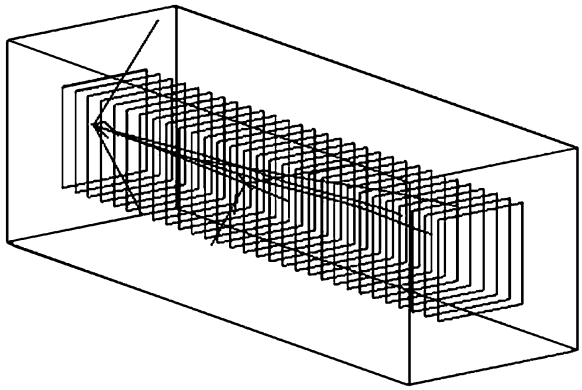

Fig. 1. Schematic representation of the phantom used in the depth-dose simulations. It is important to note the production of secondaries as a direct result of inelastic nuclear interactions of protons within the phantom.

relative isotopic abundances, of phantom materials were obtained using an ICRU based program [6].

To determine the dose as a function of depth, the energy deposited by every particle (whether this be primary or secondary) within a sensitive volume was simulated. This was achieved by tracking the energy depositions from both primary and secondary particles in each slice for a single incident proton history. These energy depositions were summed to provide the total energy deposited within the slice for a given history. Upon completion of the simulation, the total energy deposition in each sensitive slice was determined. From this information the absorbed dose deposited as a function of depth could be ascertained.

In order to determine the effect that inelastic scatter has on the depth-dose distribution, the simulation would initially be run without taking into account inelastic scatter and then again with identical parameters taking inelastic scatter into account. The depth-dose distributions for both would then be compared. This comparison was based on parameters such as the peak to entrance dose ratio, the integral dose, the Bragg peak position, and the entrance dose.

B. Results

For verification of the Monte Carlo simulation, GEANT 4 code simulations of the absorbed dose for a 160.7 MeV proton beam of σ =0.8035 MeV within a homogeneous water phantom were compared with GEANT4 simulation data supplied by H. Paganetti from the North-Eastern Proton Therapy Centre (NEPC), Massachusetts General Hospital (MGH), Boston. The simulation data supplied by Paganetti utilized the same incident beam properties. The phantom consisted of a homogeneous water tank with a 10-mm-thick Perspex lid. The GEANT4 simulation of Paganetti has undergone extensive experimental verification at NPTC and can be considered to be a good benchmark for dose distributions in water. Fig. 2 shows the relationship between both sets of data.

Excellent agreement was found between the two data series for Bragg peak position, FWHM, plateau dose and distal edge. A slight shift in the Bragg peak was observed and no verified simulation data was supplied by H. Paganetti in the first 10 mm of the distribution due to a 10-mm-thick Perspex lid situated at the start of the water tank. The shift in Bragg peak, while small, was accounted for using the differences in the relative stopping power between water and Perspex [6] for the first 10 mm. When this was applied, the peak positions were found to be almost identical. Similar verification simulations were conducted for incident protons from three independent sources with energies of 60, 200, and 250 MeV. In all cases, the GEANT4.5.2 simulation compared extremely well. As such, it can be concluded from this analysis that the Monte Carlo simulation using the GEANT4.5.2 code has undergone preliminary verification in the mean clinical energy range.

Figs. 3 and 4 show the effect of inelastic scattering on the dose distribution in different phantom materials for monoenergetic 60 and 200 MeV proton beams, respectively.

Results for both proton energies clearly demonstrated the effect of composition of the phantom on Bragg peak position (Table I). Additionally, the role of inelastic scattering can be seen in the amplitude (shape) of the Bragg peak when inelastic interactions have been taken into account in the absorbed dose simulations. This difference became much more pronounced with increasing proton energy. The results on range, the ratio of the peak-to-entrance dose for different materials, with and without inelastic scattering, are presented in Tables II and III.

It is clear from the 60 and 200 MeV results that there is indeed an effect not only on the range of the protons within the phantom as a result of the composition, but also a difference in the inelastic scatter component. In the case of the 60-MeV protons, the difference in the Bragg peak position was approximately 14 mm across the simulated materials. In the case of the 200-MeV proton beam, this effect was measured at almost 120 mm. It was established that the stopping power determined the range of the primary protons within different materials. This parameter is already included in many treatment planning systems to identify any differences in range that is encountered as a result of a heterogeneous patient geometry. However, this research highlights the importance of the inclusion of accurate geometry compositional information as errors in composition can result in large difference of the position of the Bragg Peak within the phantom or patient.

As the incident proton energy increased, the effect of inelastic scatter on the key output parameters also increased. A degradation in peak to entrance dose ratio was observed to be around a 5%–8% for 60-MeV protons and over 30% for a 200 -MeV beam. Taking into account that the inelastic cross section depends on the proton energy and the composition of the target, the effect will be dominated by different materials under different proton energies. At 60 MeV, the material displaying the greatest effect was A-150, while at 200 MeV the most effected material was muscle.

The phantom material also affects the spectra of secondary particles produced via inelastic scatter. It is clear from Table IV that when we consider the difference in integral dose, muscle has the highest discrepancy between the simulation where inelastic scatter was considered and the simulation where it was ignored. This is a direct result of muscle producing more long-range secondaries, such as neutrons and photons, which carry dose out of the sensitive slices and away from the incident protons track. These results highlight the need for the inclusion of accurate material compositions and the cross sections of

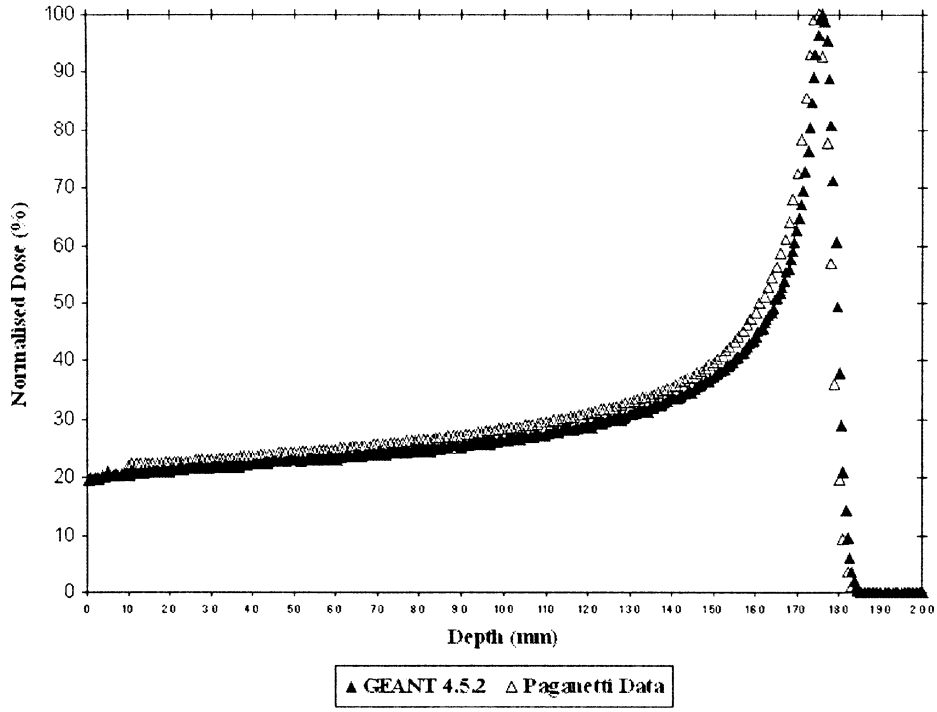

Fig. 2. Comparison of verified simulation data supplied by Dr. Paganetti and GEANT4.5.2 simulation utilized in this investigation for a 160.7-MeV proton beam incident on a water phantom.

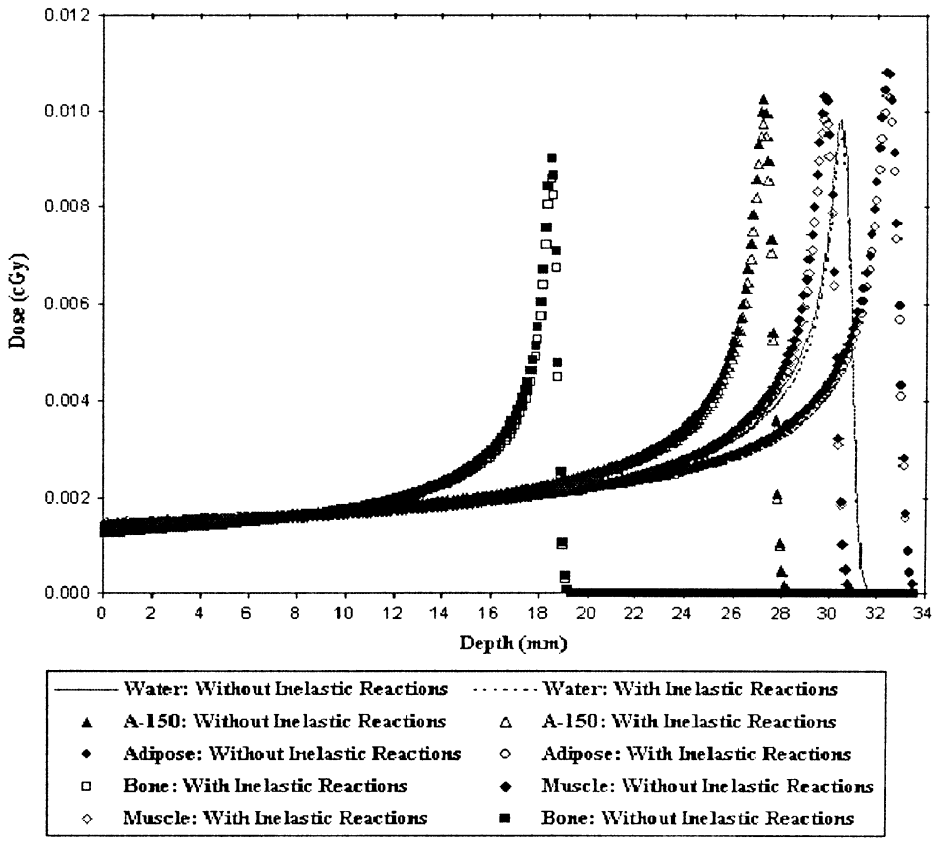

Fig. 3. Comparison of depth-dose distributions for a monoenergetic 60-MeV proton beam in different phantom materials.

inelastic reactions within the treatment planning systems. The cross sections of inelastic scatter and the spectra of secondary particles appeared to not only change between materials, but also with incident proton energy. It is important to mention that uncertainty in inelastic cross sections will effect dose distributions in phantom materials.

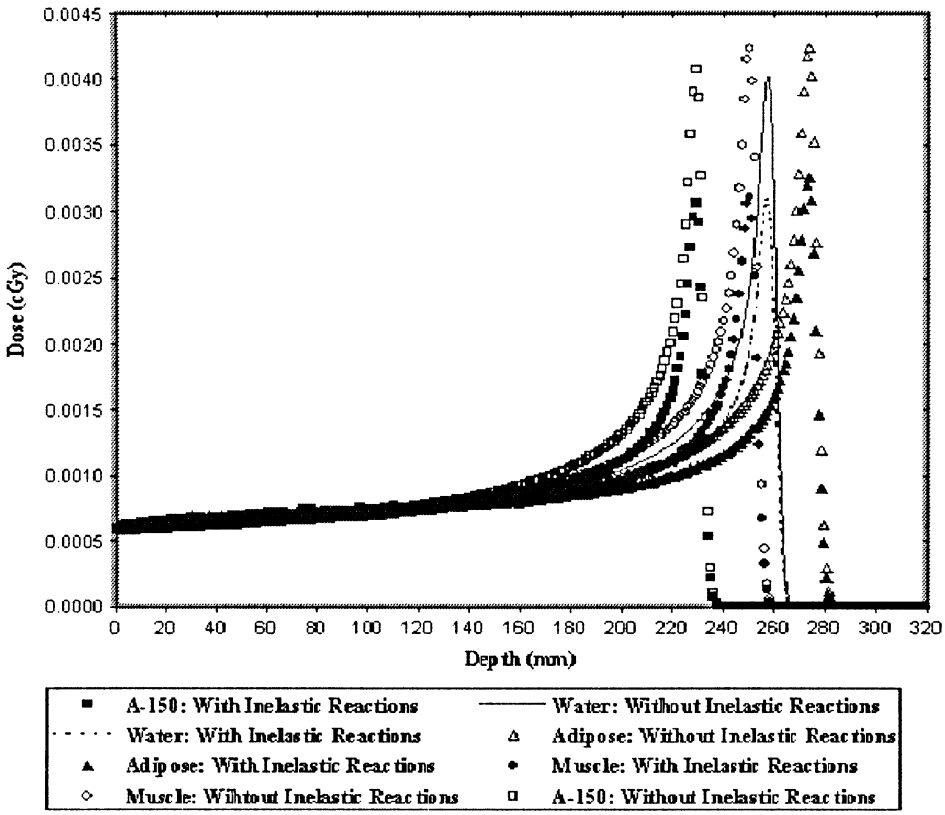

Fig. 4. Comparison of depth-dose distributions for a monoenergetic 200-MeV proton beam in different phantom materials.

TABLE I
ELEMENTAL COMPOSITIONS BY RELATIVE ABUNDANCE FOR THE MATERIALS CONSIDERED [6]

Element	Water (% by Mass)	A-150 (% by Mass)	Adipose ICRP (% by Mass)	Bone ICRP (% by Mass)	Muscle ICRP (% by Mass)
H	11.1894	10.1	11.9477	4.7234	10.0637
C	-	77.7	63.7240	14.4330	10.7830
N	-	3.5	0.7970	4.1990	2.7680
O	88.8106	5.2	23.2333	44.6096	75.4773
F	-	1.7	-	-	-
Na	-	-	0.0500	-	0.0750
Mg	-	-	0.0020	0.2200	0.0190
P	-	-	0.0160	10.4970	0.1800
S	-	-	0.0730	0.3150	0.2410
Cl	-	-	0.1190	-	0.0790
K	-	-	0.0320	-	0.3020
Ca	-	1.8	0.0020	20.9930	0.0030
Fe	-	-	0.0020	-	0.0040
Zn	-	-	0.0020	0.0100	0.0050

While it has been shown that inelastic products effect the depth-dose distribution of the therapeutic proton beam within different materials, the biological effect of these secondaries should also be taken into account utilising RBE if a biological model is part of planning system.

III. VERIFICATION OF MONTE CARLO SIMULATIONS USING SILICON MICRODOSIMETRY

If future treatment planning systems are based on full Monte Carlo simulations that provide absorbed and biological dose distributions, verification of all secondaries is an important issue for quality assurance (QA). The idea of verifying a complicated mixed radiation field in a phantom simulated by Monte Carlo using MCNP code by measurements of the absorbed dose in emended material which is different to the phantom has been proposed by Rosenfeld and implemented in epithermal boron neutron capture therapy (BNCT) [7]. This method has been used to measure the displacement kinetic energy released in a mass (KERMA) in Si, which is possible through the changing electrical parameters of a Si diode used as a measure of the cumulative effect of a mixed radiation field. For verification of Monte Carlo simulations in proton therapy, measurements of the pattern of single events of deposition energy by secondary particles will be advantageous in comparison with the measurement of a cumulative effect as in BNCT [7], [8].

TABLE II
BRAGG PEAK POSITION, THE RATIOS OF PEAK TO ENTRANCE DOSES (WITH AND WITHOUT INELASTIC SCATTER), AND THE RELATIVE DIFFERENCE IN THIS RATIO FOR 60-MeV DEPTH-DOSE DISTRIBUTIONS

Material	Bragg Peak Position (mm)	Without Inelastic Scattering	With Inelastic Scattering	Difference (%)
Water	30.3425	7.036	6.690	5.17
A-150	27.1952	7.353	6.822	7.78
Adipose	32.4425	7.569	7.136	6.07
Bone	18.4475	7.140	6.729	6.11
Muscle	29.8175	7.478	7.051	6.06

TABLE III
BRAGG PEAK POSITION, THE RATIOS OF PEAK TO ENTRANCE DOSES (WITH AND WITHOUT INELASTIC SCATTER), AND THE RELATIVE DIFFERENCE IN THIS RATIO FOR 200-MeV DEPTH DOSE-DISTRIBUTIONS.

Material	Bragg Peak Position (mm)	Without Inelastic Scattering	With Inelastic Scattering	Difference in ratio (%)
Water	257.545	6.872	5.134	33.8
A-150	229.265	6.999	5.106	37.1
Adipose	273.705	7.042	5.331	32.0
Muscle	250.475	7.128	5.141	38.6

TABLE IV
INTEGRAL DOSES WITH AND WITHOUT INELASTIC SCATTERING AND THE RELATIVE DIFFERENCE FOR 200 MeV DEPTH DOSE DISTRIBUTIONS. INTEGRAL DOSE IN CGY PER 200 000 PROTONS

Material	Without Inelastic Scattering	With Inelastic Scattering	Difference (%)
Water	0.2543	0.2362	7.7
A-150	0.2267	0.2102	7.9
Adipose	0.2775	0.2570	8.0
Muscle	0.2552	0.2278	12.0

A promising tool for this purpose could be silicon microdosimetry instrumentation, which was developed at Centre for Medical Radiation Physics, University of Wollongong, Wollongong, Australia, and tested in neutron and proton therapy applications [9]–[11]. The silicon microdosimeter is based on an array of sensitive micron-size silicon volumes in which deposited energy from each event can be measured. Silicon microdosimeters may be incorporated into the Monte Carlo calculations used by future treatment planning systems. In this situation, the role of silicon microdosimetry in proton therapy can be revised. By comparing the experimental and theoretical energy deposition spectra one can refine the model of the primary beam, components of the geometry such as beam modifying devices, the patient, the detector, or the physical models of the interaction of the former with the latter. Tissue equivalency of the detector system is not required in the proposed approach. Validation of this method was investigated at NPTC under a 230-MeV proton beam [9].

A. Method of Simulation and Experiment

The facility at NPTC uses a cyclotron to accelerate a proton beam to an initial energy of 230 MeV. The beam then passes through a range modulator filter to create the desired spread in the Bragg peak. A double scattering system using a fixed scatterer and a second nonuniform thickness scatterer produce a beam with a uniform intensity in the lateral profile over a 10×10 cm^2 field size. The microdosimeter was placed at a number of depths along the Bragg curve in a water phantom and the spectra of energy deposition events were acquired. Measurements were performed with 10-μm-thick silicon-on-insulator (SOI) devices to maximize the signal to noise ratio. These results demonstrated the high resolution of the silicon microdosimeter and the ability to operate at beam currents typically used in clinical therapy. Fig. 5 shows the dose distribution measured with an ionizing chamber and the point of measurement within the silicon microdosimeter at different depths in a water phantom.

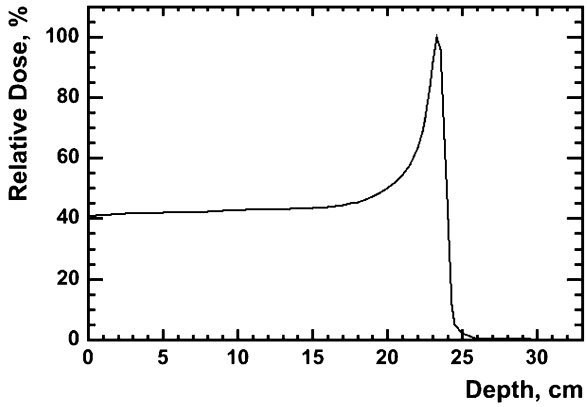

Fig. 5. Depth-dose distribution for the proton beam used in this study.

Owing to the restriction on computation times is necessary to separate the simulation of these measurements into two; the first simulated the passage of the primary beam through the beam modifying devices and calculated the distribution of transmitted proton energies. The second used the energy spectrum derived from the first to transport the beam through the phantom and microdosimeter probe.

1) Simulation of Beam Modifying Devices: A stack of right-angled parallelepiped (RPP) volumes forms a simplified model of the beam modifying devices (see Fig. 6), as follows: 1) lead beam scatterer; 2) lead range modulator; 3) carbon range modulator; 4) beam spreader; 5) transmission ion chamber; 6) nozle; 7) phantom wall is shown. The materials used in this simulation enabled an energy spectrum of the incident proton beam to be determined. The spread of the transmitted beam was simulated and a gaussian fit was determined from the simulated results. From this relationship the mean energy was estimated to be 192.4 MeV while σ =1.24 MeV and for the primary pencil beam of energy 230.5 and σ =0.41 MeV. This simulation provided the beam characteristics that would determine the parameters of the incident beam onto the phantom geometry in the second simulation.

2) Simulation of Phantom and Microdosimeter: The silicon sensitive volume was modeled as a single right-angled parallelepiped of dimensions $4800 \times 1600 \times 10$ μm^3. The charge collection efficiency was 0.8, as was derived in previous research [11]. The complicated device overlayer geometry was

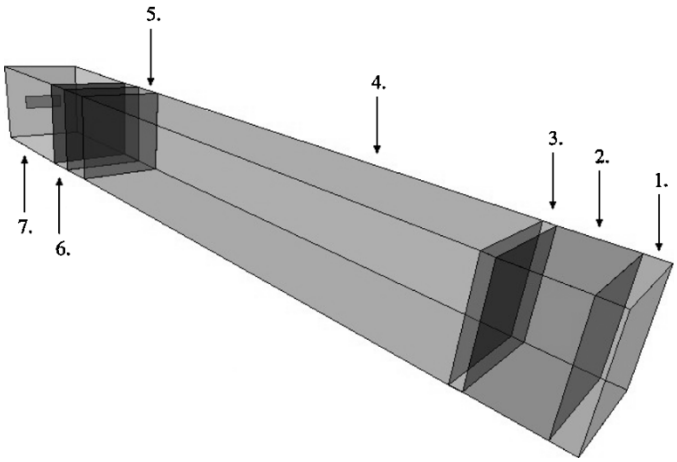

Fig. 6. Model of beam modifying devices used in GEANT4 simulation (1. lead, 1.31 mm; 2. lead, 4.52 mm; 3. graphite, 0.7753 mm; 4. water, 36.5 mm; 5. water, 3.04 mm; 6. air 2550 mm; 7. perspex, 10 mm).

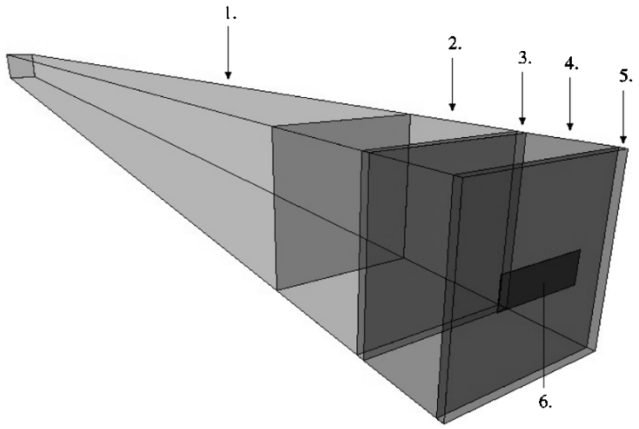

Fig. 7. Model of phantom and detector geometry used in the GEANT4 simulation (1. water phantom; 2. Perspex probe holder; 3. aluminum shield; 4. Perspex converter; 5. air gap; 6. silicon volume and overlayer).

simplified to a 1 μm thickness SiO2 layer. The 300 μm air gap between the surface of the silicon microdosimeter and the Perspex converter was also modeled, along with the 3.5-mm Perspex converter, 0.4-mm-thick aluminum shield, 6-mm probe holder, and a thickness of water corresponding to the depth of measurement. This structure is displayed in Fig. 7. Simulations were made for phantom thickness of 10, 188, 220, 227, 238, and 248 mm. The location of these depths along the bragg peak can be seen in Fig. 5 and [9]. The lateral dimensions of the water phantom and other materials were set as twice the width of the silicon sensitive volume.

The primary beam was modeled as a pencil beam that is normally incident on the surface of the phantom. This beam was assumed to have a Gaussian distribution in energy determined from the first simulation of the passage of protons through beam modifying devices. The number of protons used in each simulation was $10^6, 10^7, 10^7, 10^7, 10^7, 10^9$ for depths of measurements of 10, 188, 220, 227, 238, and 248 mm, respectively. The charged secondaries were modeled using the G4PreCompound Model and were only tracked if their residual range in material was greater than 1 μm. Electrons and gamma photons were only tracked if their residual range in the medium was greater than 10 cm.

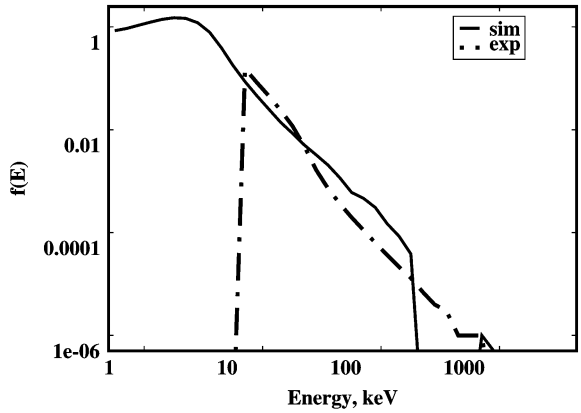

Fig. 8. Spectra of energy deposited in the silicon microdosimeter at 10-mm depth in water phantom.

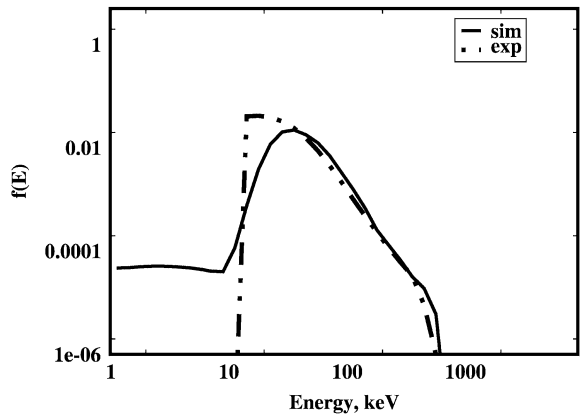

Fig. 9. Spectra of energy deposited in the silicon microdosimeter at 227-mm depth in water phantom.

If a charged particle traversed the sensitive volume of the detector the ionization energy lost in the sensitive volume was calculated. Energy lost in the sensitive volume was assumed to be equal to energy deposited and this energy deposition event was tallied. The statistics of electron hole generation were ignored.

B. Results

Figs. 8 and 9 show an example of the simulated spectra of deposited energies in the silicon microdosimeter at depths of 10 mm (entrance region) and 227 mm (Bragg peak region). These results were compared with experimentally measured data. First, the experimental results were not available below 10 keV owing to the noise threshold of the microdosimeter. Agreement between the two curves in Fig. 8 in the region 10–60 keV is evident however the two curves depart for events greater than this value. The simulation spectrum extends to energies of 500 keV whereas the experimental results extend beyond 1 MeV. This may be a result of the limited statistics available for the simulated data. The beam was considered normally incident onto the phantom and at this shallow depth the angular distribution of protons may be narrower than the actual distribution. Oblique strikes to the microdosimeter, and hence, high-energy deposition events are unlikely in this model.

In the real situation, however, the beam is not normally incident but possesses some angular distribution that would serve to broaden the angular distribution of protons at depth, increasing the occurrence of oblique strikes.

At 227 mm, the peak in the simulated results was found to shift further to higher energies as expected for reduced proton energy. In this situation, the curves agree reasonably well in the region 50–500 keV. The discrepancy between the curves exists at low values of energy deposition around 10–50 keV. It is possible that this discrepancy is associated with an underestimation of the gamma field due to simplification of the beam modification process. Discrepancies under higher deposited energies could possibly be associated with simplification of microdosimeter overlayer in thickness and in composition and angular distribution of incident protons.

IV. Conclusion

Inelastic products have been shown to be an important consideration to the depth-dose distribution of therapeutic proton beams. Different phantom materials produce different levels of inelastic scatter and different inelastic products. The spectra of secondary particles and the cross section for inelastic scatter also change as a function of energy. Thus, accurate patient geometry and the composition of this geometry needs to be accurately input into the treatment planning system along with the energy of the incident beam. Secondary radiations also need to be tracked and their effect noted. This can be achieved using Monte Carlo based treatment planning systems that utilize parallel computing techniques to provide clinically acceptable simulation times.

Simulations of energy deposition from single events of primary and secondary radiation in silicon microdosimeter measurements in proton therapy were performed using the GEANT4 Monte Carlo toolkit. Significant discrepancies were observed between simulated and experimental data. Future simulations should be performed to model the beam modifying devices in detail. This should include detailed geometry and composition of beam modifying devices and diagnostics. In this situation, the primary and secondary radiation field, particularly at shallower depths, could be more accurately modeled. Future works will be conducted in the modeling of neutron and electron contamination of beam from beam modification devices. Incorporating such a detailed model would however severely lengthen calculation time. Further work is, therefore, necessary to investigate parallel computing possibilities for Monte Carlo calculations for proton therapy.

Simulation results were analyzed to study the importance of particles originating from inelastic interactions within the silicon volume. These events were not seen to be important for a proton therapeutic beam. This means that this method can be applied accurately for verification of an external radiation field generated in a phantom, i.e., outside the silicon volume of the microdosimeter. In this situation, if the microdosimeter is to be applied to proton therapy with the aim of making tissue equivalent microdosimetric spectra, then a simple scaling factor may suffice as was proposed in [10]. This is because there is no need to subtract theoretical events contributing to microdosimetric spectra from high LET products generated within the Si sensitive volume as a result of interaction of protons with silicon.

Future experimental measurements should be performed in heterogenous phantoms with elemental compositions close to human tissue such as those provided in ICRU44. The microdosimeter probe design should be altered to remove all material surrounding the microdosimeter, with the exception of aluminum shielding.

Acknowledgment

The authors would like to thank ANSTO and AINSE for access to the cluster computing facility used for some simulations carried out for this paper. The authors would also like to thank Dr. Paganetti, NEPC, for providing simulation data on proton-absorbed dose in a water phantom from a verified simulation system, as well as Dr. R. Shulte, Loma Linda Medical Centre, for useful discussions during this work.

References

[1] H. Paganetti, "Nuclear interactions in proton therapy: Dose and relative biological effect distributions originating from primary and secondary particles," *Phys. Med. Biol.*, vol. 47, pp. 747–764, 2002.

[2] R. Kohno *et al.*, "Experimental evaluation of validity of simplified Monte Carlo method in proton dose calculations," *Phys. Med. Biol.*, vol. 48, pp. 1277–1288, 2003.

[3] N. Tilly *et al.*, "The Influence of Proton RBE Variation in Clinical Proton Beams," unpublished.

[4] S. Agostinelli *et al.*, "Geant4—A simulation toolkit," *Nucl. Instrum. Methods B*, vol. 506, pp. 250–303, 2003.

[5] *Geant4 Physics Reference Manual*, Jan. 29, 2003. Geant4 User's Documents.

[6] Nat. Inst. Standards Technol. (NIST) PSTAR Database Program [Online]. Available: http://physics.nist.gov/cgi-bin/Star/compos.pl?ap

[7] M. G. Carolan *et al.*, "Validation of Monte Carlo dose planning by epithermal beam dose distribution measurements in phantoms," in *Proc. 6th Int. Symp. Neutron Capture Therapy*, Kobe, Japan, Oct. 31–Nov. 6 1994, p. 12.

[8] M. G. Carolan, A. B. Rosenfeld, J. N. Mathur, and B. J. Allen, "Characterization and use of MOSFET gamma dosimeters and silicon PIN diode neutron dosimeters for epithermal neutron beam dosimetry," in *Advances in Neutron Capture Therapy*. New York: Elsevier, 1997, vol. V1, ISBN 0 444 827 811, pp. 192–197.

[9] A. Rosenfeld, P. Bradley, I. Cornelius, and J. Flanz, "New silicon detector for microdosimetry applications in proton therapy," *IEEE Trans. Nucl. Sci.*, vol. 47, pp. 1386–1394, Aug. 2000.

[10] P. Bradley, A. B. Rosenfeld, B. J. Allen, J. Coderre, and J. Capela, "Performance of silicon microdosimetry detectors in boron neutron capture therapy," *Radiation Res.*, vol. 151, pp. 235–243, 1998.

[11] P. D. Bradley, A. B. Rosenfeld, and M. Zaider, "Solid state microdosimetry," *Nucl. Instrum. Methods B*, vol. 184, pp. 135–157, 2001.